Mechanical Technology and Engineering Insights

www.mtei.reapress.com

Mech. Technol. Eng. Insights. Vol. 2, No. 4 (2025) 294–314.

Paper Type: Original Article

Influences of Constitutive Models and Strain Path on Predicted Forming Limit Curves for AA5182-0 Alloy

Ali Basti[1,*], Soheila Sojodi[1], Seyed Reza Falahatgar[1], Seyedeh Maryam Mirfalah Nasiri[1]

[1] Department of Mechanical Engineering, University of Guilan, Rasht, Iran; basti@guilan.ac.ir; soheila_sojodi@yahoo.com; falahatgar@guilan.ac.ir; Mirfalah@gmail.com.

Citation:

Received: 23 February 2025 *Revised: 14 April 2025* *Accepted: 12 June 2025*	Basti, A., Sojodi, S., Falahatgar, S. R., Mirfalah Nasiri, S. M. (2025). Influences of constitutive models and strain path on predicted forming limit curves for AA5182-0 alloy. *Mechanical Technology and Engineering Insights*, *2*(4), 294-314.

Abstract

The onset of necking in a metal forming process is usually predicted by the Forming Limit Curve (FLC). Different hardening laws and yield criteria are employed to describe the plastic behavior of the AA5182-0 aluminum sheet, and their constant parameters are determined. Results indicated that the calculated FLC based on the modified Kim-Tuan and Yld2000-2d yield function can predict the experimental data better than other models. Because of the complexity of the metal forming process, the loading path is rarely linear; therefore, forming limits should be computed in nonlinear strain path conditions. Theoretical FLCs show that the strain path has a notable influence on the limit strains, and the path dependency of the Forming Limit Stress Curve (FLSC) is much less than limit curves in strain space. It was found that in multistep loading processes, limit stresses are affected by strain path when the pre-effective strain reaches a critical value, and this value is sensitive to selected constitutive models. Therefore, the material description has a considerable effect on the path dependency of forming limit stresses. Consequently, at the end of this study, the effects of hardening models and yield functions on the sensitivity of the FLSC to strain path are examined.

Keywords: Forming limit curve, Different hardening laws, Yield criteria, Nonlinear strain path, Forming limit stress curve.

1 | Introduction

In the metal forming process, knowing the maximum allowable strains before necking is an important issue. For this purpose, forming limit curves play an important role in the analysis of the sheet metal process and

Corresponding Author: basti@guilan.ac.ir
https://doi.org/10.48313/mtei.v2i4.75
Licensee System Analytics. This article is an open-access article distributed under the terms and conditions of the Creative Commons Attribution (CC BY) license (http://creativecommons.org/licenses/by/4.0).

are an appropriate tool to evaluate the metal formability. This Diagram, which is in principal strain space, is established to predict the necking in sheet metal forming processes.

Conventional FLC was initially presented by Keeler [1], and it was developed by Goodwin [2]. Since experimental extraction of the FLC entails exact experiments and demands a considerable amount of time and money, extensive research is conducted to calculate and plot the diagrams using analytical methods.

In the theoretical methods, the M-K instability theory proposed by Marciniak and Kuczynski is the most widely used criterion to determine the forming limits of sheet metals. Marciniak and Kuczynski considered the geometrical defects in the material, so they developed the M-K method based on the existence of the groove in the workpiece [3].

In the M-K instability approach, the constitutive models of the material affect the prediction of the forming limit curve; therefore, there are a lot of requests to employ the exact hardening model and yield function to obtain the forming limits.

Butuc et al. [4] calculated the BBC2000, Yld96 coefficients for an aluminum alloy sheet, and they used the Newton-Raphson method to identify the constant parameters of yield functions. Also, they investigated the influences of different yield criteria on the calculated forming limit strains.

Wu et al. [5] studied the anisotropic behavior of the aluminum alloys experimentally. They determined the parameters of Yld91, Yld96, and K&B93 for AA5182-0 and AA3104-H19 alloys, and the forming limits computed by these functions are compared with experimental results.

Barlat et al. [6] proposed the Yld2000-2d non-quadratic yield function as a suitable criterion for describing the anisotropic behavior of sheet metals, especially aluminum alloys. Also, they determined the anisotropic coefficients of the Yld2000-2d for AA2090-T3 and AA6022-T4. Ganjiani and Assempour [7] developed the M-K theory to calculate the FLC of the AK steel and AA5XXX alloys. Also, they used Hosford and BBC2008 yield functions by considering the Voce and power hardening models to describe the mechanical behavior of alloys.

Pham et al. [8] analyzed the effects of different hardening equations to compute the FLC of aluminum alloys, and the remarkable accuracy in predicting the forming limits was observed when applying the Kim-Tuan model. Then, their advanced Kim–Tuan hardening law was introduced to improve the accuracy of the post-necking behavior for a commercial pure titanium alloy. Also, a procedure was developed to identify the constant parameters of the proposed hardening model and YLD2000-2d using a curve fitting method [9].

Mirfalah-Nasiri et al. [10], [11] applied different yield functions, including Yld96, K–B, and Yld2011-18p, to compute the limit strains, and also they analyzed the influences of the normal stress and shear stress on the forming limits of AA3104-H19 aluminum alloy. It was concluded that the Yld2011-18p can estimate the limit strains better than K-B and Yld96.

Hou et al. [12] employed Ludwik, Swift, and Ghosh hardening models to describe the plastic behavior of the AL5182-H111 sheet, and results showed that the Ghosh law is the most accurate model for predicting the limit strains. The influences of the various yield criteria were investigated to estimate the forming limit strains at cryogenic temperature by Wang et al. [13], and it was indicated that Yld2000–2d is an appropriate yield criterion to express the yield behavior of the 2024-O aluminum alloy.

Uppaluri and Helm [14] developed direct and inverse procedures to calculate the coefficients of the Gotoh fourth-order polynomial yield function. By comparing the experimental data and the theoretically obtained results, it was proved that both parameter identification approaches are successful in describing the yield behavior of the aluminum and steel alloys.

The experimental data and theoretical analysis demonstrated that the conventional FLC was highly sensitive to the strain path. Considering the path independence of the forming limit curves is a serious requirement in industrial applications. Many studies have been done to understand the nature of the path dependence of forming limits with both experimental and theoretical methods.

Graf and Hosford [15] investigated the effect of nonlinear strain paths on the forming limits of aluminum alloys through careful experiments for the workpieces that are pre-strained along different stress ratios. It was concluded that the change of the strain path has a great effect on the specimen's formability. Yoshida et al. [16] discussed the path dependence of the limit stresses during different loading paths based on a phenomenological plasticity theory. It was expressed that the path independence of the Forming Limit Stress Curve (FLSC) is due to the isotropic hardening behavior that is related to the constitutive model of the material.

Yoshida and Kuwabara [17] computed the FLC and FLSC for a steel tube under linear and bilinear loading paths. The results indicated that the limit stresses are not path independent, and the path dependence of FLSC is affected by the hardening behavior of the material. Nurcheshmeh and Green [18] investigated the path dependency of the FLSC for various combined loading histories, and it was observed that for a range of pre-strain values, the FLSC remains constant along different paths.

Wang et al. [19] determined the forming limit diagram under four nonlinear strain paths experimentally and theoretically, and the effects of the loading path on forming limit curves are discussed. Their investigations were carried out based on the Chaboche hardening law and Yld2000-2d yield function.

Zhalehfar et al. [20] surveyed the influences of different pre-strains on the forming limit diagram of AA5083 alloy in bilinear strain path processes. Results show that the sensitivity of the FLSC to pre-strain is less than that of FLC, and limit stresses are suitable criteria to use in bilinear loading path processes.

Sojodi et al. [21] investigated the influence of the compressive normal stress on the path dependence of FLSC by applying various hardening equations. Also, they examined the effect of the pre-strain magnitudes on the sensitivity of FLC to compressive normal stress.

In this paper, the effect of the nonlinear loading path on forming limits by considering different hardening models and various yield functions is studied. Swift, Kim-Tuan, and modified Kim-Tuan work hardening laws are applied to estimate the stress-strain curve of the AA5182-0 aluminum alloy. The Gotoh and Yld2000-2d yield criteria are used for prediction the yield behavior of the sheet, and constant parameters of all constitutive relationships are computed. Theoretical limit strains in linear strain path condition according to different material models are plotted and compared with the test data in [5], and the most accurate model is chosen.

Then, the influences of the loading path on the forming limit diagrams are studied, and the path dependence of FLC and FLSC is analyzed in detail. At the end, the sensitivity of the FLSC to the magnitude of the pre-strain for different hardening models and yield functions is discussed ,and the critical effective strain values that specify the path dependence of FLSC for various constitutive models are determined.

2 | Mechanical Properties

2.1 | Yield Functions

Because of the anisotropic property of aluminum sheets in the cold rolling process, the suitable yield function has a significant effect on the precision of the FLC. This study compares the effect of the Hill48, Gotoh, and Yld2000-2d yield criteria on predicting the yield behavior of the AA5158-0 aluminum alloy. Their constant parameters are determined according to the values of the r-value and yield stress along different grooves from the rolling direction. These material anisotropic parameters are presented in *Table 1*.

Table 1. Yield stress and r-value of AA5182-0 alloy in different directions [5].

σ_0 MPa	σ_{45} MPa	σ_{90} MPa	σ_b MPa	r_0	r_{45}	r_{90}	r_b
120	116.41	118.26	118.31	0.72	0.90	0.84	0.87

2.1.1 | Hill48 yield criterion

Hill48 criterion is one of the simplest and most common yield functions to describe the anisotropic material behaviors, and its constant parameters are determined with explicit formulas. The formulation of the Hill48 yield function is expressed as [22]:

$$\overline{\sigma}^2 = F(\sigma_y - \sigma_z)^2 + G(\sigma_z - \sigma_x)^2 + H(\sigma_x - \sigma_y)^2 + 2(L\sigma_{yz}{}^2 + M\sigma_{zx}{}^2 + N\sigma_{xy}{}^2). \qquad (1)$$

For plane stress conditions, Hill48 is as follows:

$$\overline{\sigma}^2 = (G + H)\sigma_x{}^2 - 2H\sigma_x\sigma_y + (F + H)\sigma_y{}^2 + 2N\sigma_{xy}{}^2, \qquad (2)$$

where F, G, H, and N are material coefficients for the Hill48 yield function that are determined by using the r-value in different directions. The relations to compute the Hill48's constant parameters are given in the appendix, and these values are listed in *Table 2*.

Table 2. The anisotropic parameters of the Hill48 yield function for 5182-0 alloy.

F	G	H	N
0.4983	0.5814	0.4186	1.5116

2.1.2 | Gotoh yield criterion

Because of the Hill48 equation limitations discussed in the current section, the polynomial-type yield function was proposed by Gotoh. This fourth-order polynomial yield function is applicable to predict the yield behavior of the materials under plane stress conditions. Gotoh's yield function is expressed as [23]:

$$\overline{\sigma}^4 = A_1\sigma_x{}^4 + A_2\sigma_x{}^3\sigma_y + A_3\sigma_x{}^2\sigma_y{}^2 + A_4\sigma_x\sigma_y{}^3 + A_5\sigma_y{}^4 + (A_6\sigma_x{}^2 + A_7\sigma_x\sigma_y + A_8\sigma_y{}^2)\sigma_{xy}{}^2 + A_9\sigma_{xy}{}^4. \qquad (3)$$

A_1 to A_9 are material parameters for the Gotoh yield function that are obtained by using the direct approach as stated in the appendix. The constant parameters of the Gotoh yield function are listed in *Table 3*.

Table 3. The anisotropic parameters of the Gotoh yield function for AA5182-0 alloy.

A_1	A_2	A_3	A_4	A_5	A_6	A_7	A_8	A_9
1	-1.6744	2.6086	-1.936	1.0602	6.131	-5.2517	6.5128	9.6164

2.1.3 | Yld2000-2d yield criterion

It is widely reported that the YLD2000-2d is a proper yield criterion to describe the anisotropic yield behavior of the aluminum sheets [6]. For this yield function, the formulation is expressed as:

$$\phi = \phi' + \phi'' = 2\overline{\sigma}^m, \qquad (4)$$

where $\overline{\sigma}$ is equivalent stress and m is the constant value that for FCC metals, m=8. Functions ϕ' and $\phi''$are obtained as below [24]:

$$\phi' = |X'_1 - X'_2|^m,$$
$$\phi'' = |2X''_2 + X''_1|^m + |2X''_1 + X''_2|^m. \qquad (5)$$

X'_i and X''_j (i, j=1,2) are the principal values of the matrix X' and X'', and are expressed as:

$$X'_i = \frac{1}{2}(X'_{11} + X'_{22} \pm \sqrt{(X'_{11} - X'_{22})^2 + 4X'^2_{12}}\,), \qquad (6)$$

$$X_i'' = \frac{1}{2}\left(X_{11}'' + X_{22}'' \pm \sqrt{(X_{11}'' - X_{22}'')^2 + 4X_{12}''^2}\right).$$

Components of X' and X'' are obtained as:

$$X' = L'\sigma,$$
$$X'' = L''\sigma, \tag{7}$$

where L' and L" are linear transformation tensors that are calculated by eight constant parameters as follows:

$$\begin{bmatrix} L_{11}' \\ L_{12}' \\ L_{21}' \\ L_{22}' \\ L_{66}' \end{bmatrix} = \begin{bmatrix} 2/3 & 0 & 0 \\ -1/3 & 0 & 0 \\ 0 & -1/3 & 0 \\ 0 & 2/3 & 0 \\ 0 & 0 & 1 \end{bmatrix} \begin{bmatrix} \alpha_1 \\ \alpha_2 \\ \alpha_7 \end{bmatrix}. \tag{8}$$

$$\begin{bmatrix} L_{11}'' \\ L_{12}'' \\ L_{21}'' \\ L_{22}'' \\ L_{66}'' \end{bmatrix} = \frac{1}{9}\begin{bmatrix} -2 & 2 & 8 & -2 & 0 \\ 1 & -4 & -4 & 4 & 0 \\ 4 & -4 & -4 & 1 & 0 \\ -2 & 8 & 2 & -2 & 0 \\ 0 & 0 & 0 & 0 & 9 \end{bmatrix} \begin{bmatrix} \alpha_3 \\ \alpha_4 \\ \alpha_5 \\ \alpha_6 \\ \alpha_8 \end{bmatrix}. \tag{9}$$

α_1 to α_8 are eight anisotropic parameters which could be computed by eight mechanical properties of sheet metals measured experimentally [25]. The six data are r values and flow stresses in $0°, 45°$, and $90°$ direction from rolling ($r_0, r_{45}, r_{90}, \sigma_0, \sigma_{45}, \sigma_{90}$), and the other two input data are the balanced biaxial r value and flow stress($, r_b, \sigma_b$). Yld2000-2d yield function coefficients are presented in *Table 5*, and the relations to calculate α_1 to α_8 are given in the appendix.

Table 4. Parameters to determine the Yld2000-2d [25].

Direction	J	γ_j	δ_j	q_{xj}	q_{yj}
0°	1	$2/3$	$-1/3$	$1 - r_0$	$2 + r_0$
90°	2	$-1/3$	$2/3$	$2 + r_{90}$	$1 - r_{90}$
Balanced biaxial	3	$-1/3$	$-1/3$	$1 + 2r_b$	$2 + r_b$

Table 5. The anisotropic parameters of the Yld2000-2d yield function for AA5182-0 alloy.

α_1	α_2	α_3	α_4	α_5	α_6	α_7	α_8
0.9473	1.0314	0.9789	1.0136	1.0233	1.0301	1.0200	1.0678

In order to examine the accuracy of the computed coefficients for the above yield functions, the yield surface of each criterion is plotted.

Fig. 1 shows the yield surface predicted by different yield criteria and available experimental data in [5] plane stress conditions. However, Gotoh and Yld2000-2d functions effectively matched the test data; a slight deviation is seen in the yield surface based on the Hill 48 function in *Fig. 1*.

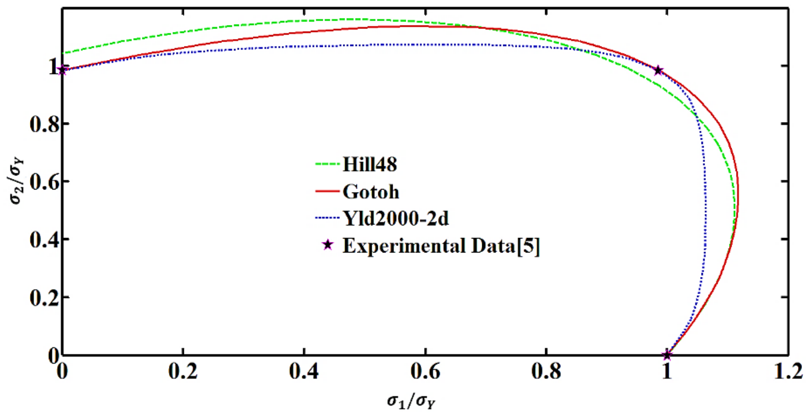

Fig. 1. Comparison of Yield surfaces based on different yield criteria and test data.

In addition, *Fig. 2* shows the comparison between the computed normalized yield stresses and r-value with the test results. The variation of these values with respect to the angle from rolling direction (θ) is computed by using the following formulas [26]:

$$\sigma_x = \sigma_\theta \cos^2\theta, \qquad \sigma_y = \sigma_\theta \sin^2\theta, \qquad \sigma_{xy} = \sigma_\theta \cos\theta \sin\theta. \tag{10}$$

$$\frac{\sigma_\theta}{Y} = \frac{1}{\bar{\sigma}(1,\theta)}. \tag{11}$$

$$r_\theta = -\frac{\sin^2\theta \frac{\partial\bar{\sigma}}{\partial\sigma_x} - \frac{1}{2}\sin 2\theta \frac{\partial\bar{\sigma}}{\partial\sigma_{xy}} + \cos^2\theta \frac{\partial\bar{\sigma}}{\partial\sigma_y}}{\frac{\partial\bar{\sigma}}{\partial\sigma_x} + \frac{\partial\bar{\sigma}}{\partial\sigma_y}}. \tag{12}$$

As depicted in *Fig. 2a*, all yield functions successfully estimated the r-value of the aluminum AA5182-0. Although Hill48 calculates the r-value with good accuracy, the prediction of the normalized yield stress is significantly distorted, as shown in *Fig. 2a*. According to the results observed in *Fig. 1* and *Fig. 2*, Gotoh and Yld2000-2d provided good accuracy in predicting the yield condition.

In contrast, the values predicted by the Hill48 function have a large deviation from experimental results, and this means Hill48 cannot be close to the real yield condition. Therefore, in the next sections of this paper, the Gotoh and Yld2000-2d yield functions are used to plot the forming limit curve of the AA5182-0 sheet.

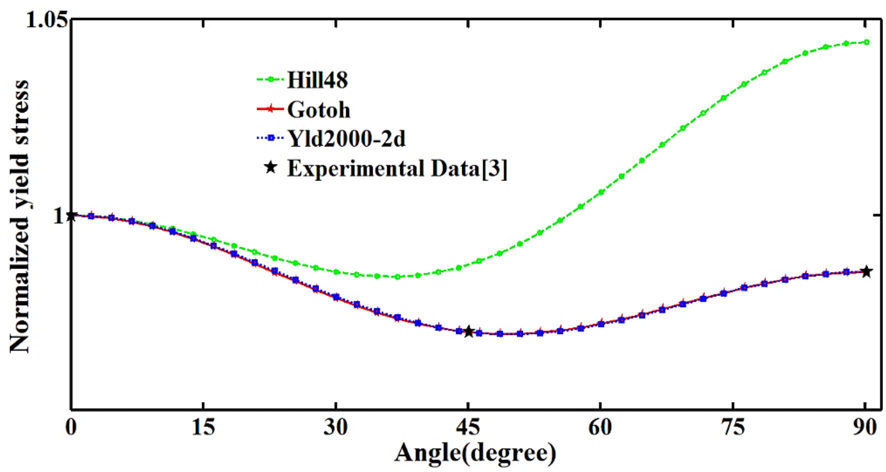

a.

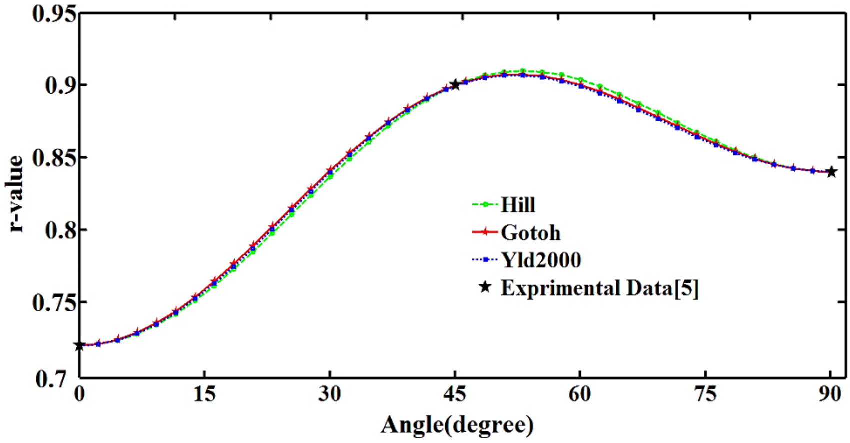

b.

Fig. 2. Comparison of test data and theoretical; a. normalized yield stress, and b r-value based on different yield criteria.

2.2 | Strain Hardening Models

For evaluating the influence of the hardening law on the FLC, Swift, Kim-Tuan, and modified Kim-Tuan relationships are utilized to describe the mechanical behavior of the AA5182-0 sheet. In the current research, the constant parameters of strain hardening models were computed by using the curve fitting method [8]. This technique was utilized to minimize the difference between stress-strain curves predicted by hardening models and the experimental data obtained from the uniaxial tensile test in [5]. The calculated parameters of hardening laws for AA5182-0 are listed in *Table 6*, and the strain hardening models are defined as follows.

Table 6. Material coefficients of the different hardening models for AA5182-0.

Hardening model	Parameter 1	Parameter 2	Parameter 3	Parameter 4	Parameter 5	Parameter 6	Parameter 7
Swift	K_s(Mpa) 499.3	ε_0 0.0075	n_s 0.2662				
Kim-Tuan	σ_0(Mpa) 123	ε_0 0.0075	σ^* 339.12	ε^* 0.21	t_K 25	h_K 0.32	K_K 360.64
Modified Kim-Tuan	S(Mpa) 97	ε_0 0.0075	ε^* 0.21	K_{mk} 360.64	a_{mk} 1.31	h_{mk} 0.58	t_{mk} 4.19

2.2.1 | Swift hardening law [22]

$$\bar{\sigma} = K_s(\bar{\varepsilon} + \varepsilon_0)^{n_s}, \tag{13}$$

where K_s and n_s are material constants for Swift work hardening. $\bar{\varepsilon}$ is the effective strain in the plastic region, and ε_0 is a constant representing the elastic strain to the yield point. The Swift coefficients for the AA5182-0 alloy are given in *Table 6*.

2.2.2 | Kim-Tuan hardening law: This strain hardening model is proposed by combining the Swift and Voce formulas. Kim-Tuan model is defined as follows [8]:

$$\bar{\sigma} = \sigma_0 + K_k[1 - \exp(-t_k\varepsilon)](\varepsilon + \varepsilon_0)^{h_k}], \tag{14}$$

where K_k, t_k, and h_k are the material constants, and σ_0 is the initial yield strength. The coefficients of the Kim-Tuan hardening model are computed according to the appendix relations and listed in *Table 6*.

2.2.3 | Modified Kim-Tuan hardening law

This advanced strain hardening model, which describes the isotropic-distortion behavior of aluminum and titanium sheet metal, is expressed as [9]:

$$\bar{\sigma} = +K_{mk}(\varepsilon + \varepsilon_0)^{h_{mk}}\left(1 + \frac{a_{mk}}{1 + \exp(t_{mk}(\bar{\varepsilon} - \varepsilon^*))}\right), \tag{15}$$

where S, K_{mk}, h_{mk}, a_{mk}, t_{mk}, and ε^* are modified Kim-Tuan equation coefficients, which are presented in *Table 6*.

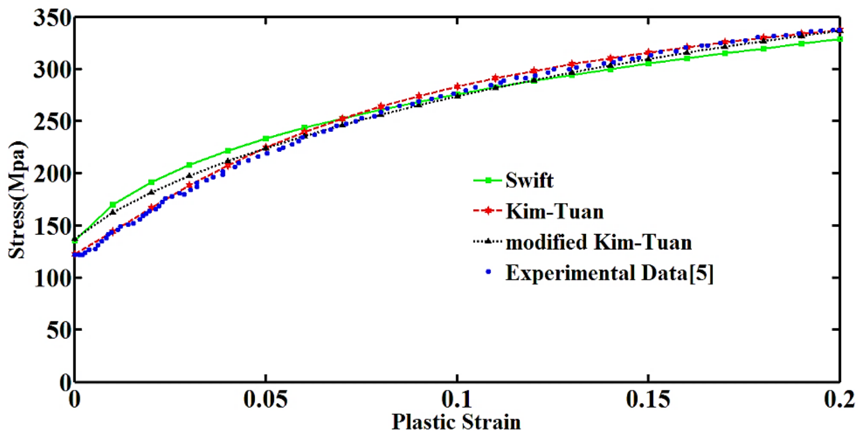

Fig. 3. Comparison of the experimental and theoretical stress-strain curves for AA5182-0 sheet.

Fig. 3 indicates the comparison between Swift, Kim-Tuan, and modified Kim-Tuan stress-strain curves and available experimental data to validate the strain hardening relationships and their constant parameters. The curve fitting technique is the most popular method for identifying the coefficients of the hardening model to decrease the difference between the predicted flow stresses and experimental results. As shown in *Fig. 3*, by fitting the hardening equations to the test data under uniaxial tensile test, it can be observed that almost all models can estimate the experimental flow stress and give satisfactory accuracy to the test result. However, it will be seen that these hardening models show different results for forming limits in the next sections.

3 | M-K Theory to Predict the FLC

One of the most popular instability criteria, which is used widely to predict the onset of localized deformation, was proposed by Marciniak and Kuczynski [3] and is now commonly known as the M-K theory. This method is based on the initial imperfection that is characterized by the reduction of thickness in a part of the sheet. The initial thickness imperfection (f_0) is defined as a long groove, as shown in *Fig. 4*, and expressed as:

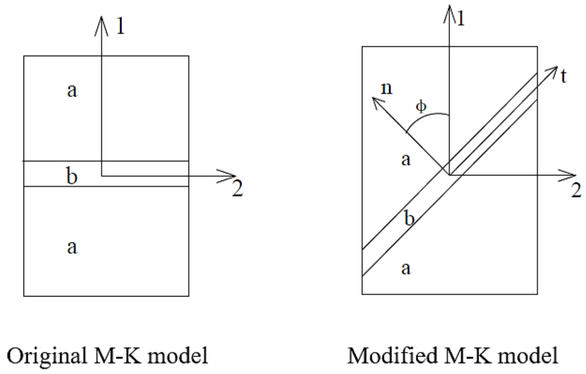

Fig. 4. The M-K instability models.

$$f_0 = \frac{t_0^b}{t_0^a}, \tag{16}$$

where t_0^a and t_0^b are the initial thickness in the safe region: 1) and defect region, and 2) respectively. In the original M-K theory, the angle of the groove is perpendicular to the principal axis-1 ($\phi_0 = 0$). The original M-K method, which neglects the groove orientation, was only proposed to determine the limit strains on the right side of the forming limit diagram. Therefore, to calculate the forming limits in the negative minor strain region of the Diagram by the M-K instability method, the effect of the initial groove angle must be considered. As shown in *Fig. 4*, to estimate the whole FLC of sheet metal, the M-K model was modified in the way that the initial groove is inclined at an angle ϕ_0 with regard to the principal axis-1.

In the M-K approach, the equivalent strain increment $d\bar{\varepsilon}^a$ with a specific stress ratio ($\alpha = \sigma_{22}^a/\sigma_{11}^a$) was applied to the safe region, and then the other strain and stress component values in this area were computed by using the flow rule, hardening equation, and yield function [21]. The unknown parameters in the groove zone were calculated according to three major assumptions, including compatibility condition, force equilibrium, and geometrical imperfection, which were expressed as:

$$d\varepsilon_{tt}^a = d\varepsilon_{tt,}^b \tag{17}$$

$$\begin{cases} \sigma_{nn}^a t^a = \sigma_{nn}^b t^b \\ \sigma_{nt}^a t^a = \sigma_{nt}^b t^b \end{cases} \Rightarrow \begin{cases} \sigma_{nn}^b = \sigma_{nn}^a/f \\ \sigma_{nt}^b = \sigma_{nt}^a/f \end{cases}. \tag{18}$$

The imperfection factor f, which is a significant factor in M-K instability theory, should be updated in every step based on the following:

$$f = \frac{t^b}{t^a} = f_0 \exp(\varepsilon_3^b - \varepsilon_3^a), \tag{19}$$

where t is the sheet thickness, and ε_3 is the strain along the thickness, which is obtained by considering the incompressibility condition. Besides, when a small increment of principal strain $d\varepsilon_{11}$ is applied in the safe region, the groove direction will change according to:

$$\tan(\phi + \Delta\phi) = \frac{1 + d\varepsilon_{11}^a}{1 + d\varepsilon_{22}^a} \tan\phi. \tag{20}$$

The numerical Newton-Raphson method is used to solve the nonlinear set of equations, and the unknown stress and strain components in the defect region are obtained when the effective strain increment in the groove reaches ten times greater than the perfect area ($d\bar{\varepsilon}^b/d\bar{\varepsilon}^a \geq 10$) [27]. This numerical procedure in each strain ratio is repeated for different groove directions to determine the minimum limit strains.

4 | Results and Discussions

4.1 | Forming Limit Evaluation

In this section, to validate the models, the predicted FLC in linear loading path conditions was compared with the corresponding experimental FLC for AA5182-0 aluminum alloy, and the effect of different hardening relationships and yield equations on the theoretical limit strains is investigated. Then, the forming limit diagram in multistep loading path conditions is plotted, and the influences of the pre-strain along different loading paths on limit strains are examined.

4.1.1 | Effects of constitutive models on the FLC

During the last decades, a lot of studies reported the effect of various constitutive models on the accuracy of the predicted FLC. In this section, to investigate the effects of material models on theoretical forming limits, Gotoh and Yld2000-2d yield functions are employed, and also the influences of the Swift, Kim-Tuan, and modified Kim-Tuan stress-strain relationships are examined. The M-K instability theory, by considering the initial groove angle and imperfection ratio $f_0 = 0.999$, is utilized to estimate the forming limit diagram in the linear loading path condition.

Fig. 5 indicates the comparison between the FLC predicted by different hardening models based on the Yld2000-2d yield function and experimental data for AA5182-0 alloy. As can be seen in *Fig. 5*, the predicted FLC according to all hardening models is in good agreement with experimental results. On the left side of the Diagram, forming limits based on the Swift and Modified Kim-Tuan hardening models are almost at a similar level of accuracy, and their results are in better agreement with the experimental data than those predicted by the Kim-Tuan. The Kim-Tuan model underestimates the forming limit strains for AA5182-0 alloy when the strain ratio is negative. The reasons for this behavior of the hardening laws are explained in detail in [21].

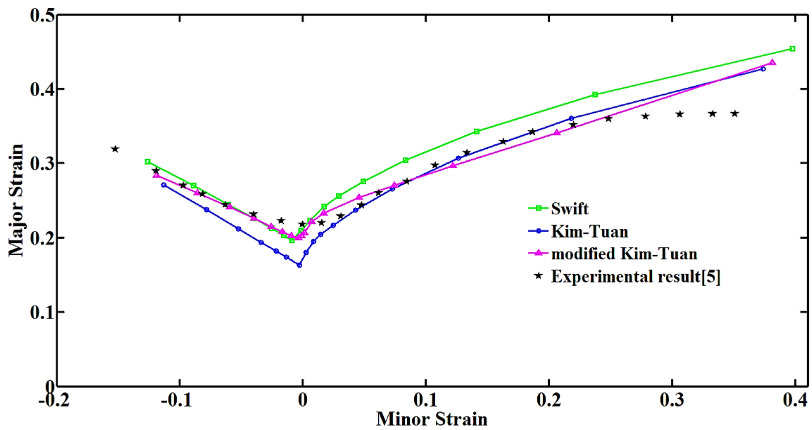

Fig. 5. Theoretical FLCs based on the Yld2000-2d yield function and experimental results for AA5182-0 sheet.

On the right side of the Diagram, the Swift hardening model overestimates the limit strains. At the same time, the calculated FLCs according to both the Kim-Tuan and modified Kim-Tuan relationships demonstrate an acceptable accuracy for the formability of AA5182-0. As illustrated in *Fig. 5*, Swift and modified Kim-Tuan can predict the FLC0, FLC in the plane strain condition, with better accuracy than the Kim-Tuan model. Results indicate that the modified Kim-Tuan model can predict almost all parts of the DiagramDiagram better than the Swift and Kim-Tuan models. Therefore, the modified Kim-Tuan strain hardening law that describes the isotropic-distortion behavior of sheet metal [9] is the proper model to predict the formability of AA5182-0 sheets by using the Yld2000-2d. To prove the above results, the absolute error for predicted limit strains is measured by using the following equation:

$$\mathrm{err}(\%) = \frac{\left|\varepsilon_1^{\mathrm{cal}} - \varepsilon_1^{\mathrm{exp}}\right|}{\varepsilon_1^{\mathrm{exp}}} \times 100, \tag{21}$$

where $\varepsilon_1^{\mathrm{exp}}$ and $\varepsilon_1^{\mathrm{cal}}$ are experimental and predicted major strain, respectively. The calculated errors are presented in *Table 7*. As indicated in *Table 7*, the modified Kim-Tuan hardening model can predict the most accurate limit strains by applying the Yld2000-2d yield function for AA5182-0 alloy.

Table 7. The computed error for major strain for different hardening models by applying the Yld2000-2d yield function.

Error	Left Side of Diagram (%)	Right Side of Diagram (%)	Whole the Diagram (%)
Swift model	2.50	11.72	9.30
Kim-Tuan model	9.20	4.90	6.03
modified Kim-Tuan model	2.55	5.03	4.38

In the continuation of this section, the theoretical FLC of AA5182-0 aluminum alloy under linear loading path is calculated according to the Gotoh yield function by using the Swift, Kim-Tuan, and modified Kim-Tuan work hardening models. As illustrated in *Fig. 6*, the Swift and modified Kim-Tuan models verified the experimental data only in the vicinity of the plane strain state, and the FLC predicted by the Kim-Tuan model almost does not match the experimental data. A Comparison of results between *Fig. 5* and *Fig. 6* proves that, however, both Gotoh and Yld2000-2d yield functions describe the yield behavior of the AA5182-0 accurately according to *Fig. 1* and *Fig. 2*, the forming limit diagram predicted by Gotoh is not appropriate, and the computed FLCs by it are poor.

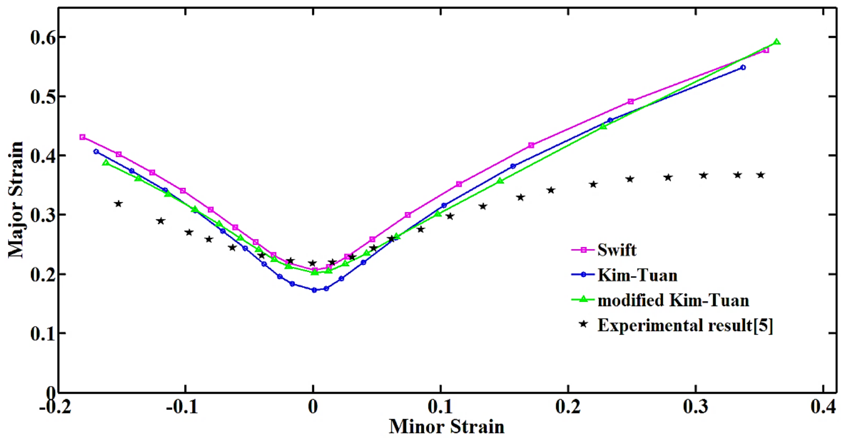

Fig. 6. Theoretical FLCs based on the Gotoh yield function and experimental results for AA5182-0 sheet.

According to the above explanation, the Yld2000-2d criterion is a suitable yield function to determine the limit strains for aluminum alloys. Also, according to *Fig. 5*, the modified Kim-Tuan strain hardening law shows the best prediction based on the Yld2000-2d for AA5182-0 sheets. For this reason, in the next section, the modified Kim-Tuan hardening law and the Yl2000-2d non-quadratic anisotropic yield function are utilized together to compute the forming limit diagrams.

4.1.2 | Effects of various pre-strains on the FLC

The M-K criterion code was developed to calculate the theoretical forming limit diagram of AA5182-0 under combined loading paths. This modified approach was used to analyze FLCs of AA5182-0 aluminum alloy sheet for a variety of nonlinear strain paths that consist of two loading stages. In multi-stage loading processes, the first stage has different magnitudes of pre-strain along the following modes: uniaxial tension ($\rho = -0.5$), plane-strain tension ($\rho = 0$), and equi-biaxial tension ($\rho = 1$). In the second stage, FLC was determined following the previous pre-strain by considering a series of linear paths in the range between uniaxial tension and equi-biaxial tension ($-0.5 \leq \rho \leq 1$).

Fig. 7 shows the forming limit diagrams obtained by combining the modified Kim-Tuan work hardening law and Yld2000-2d yield function in the bilinear strain path condition. To study the influences of different strain paths on the limit strains, the FLCs were plotted under various pre-strains along the uniaxial tension, plane strain, and equi-biaxial tension paths. In *Fig. 7*, the curves with square markers show the effect of 0.1 and 0.2 pre- effective strains in the uniaxial tension direction on the FLC. Compared to the forming limits under the linear path, this pre-strain enhances and improves the formability of the positive minor strains, but moves the left side of the curve downward; also, the pre-strain shifts the Diagram towards the negative minor strains.

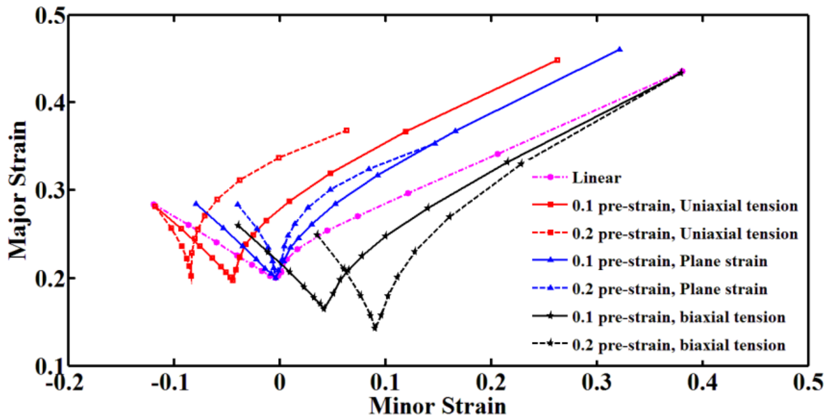

Fig. 7. The FLCs based on different pre-strains along uniaxial tension ($\rho = -0.5$), plane strain direction ($\rho = 0$), and equi-biaxial tension ($\rho = 1$).

The curves with a triangle marker in *Fig. 7* indicate the calculated forming limit diagrams after ε_1 =0.1 and 0.2 pre-strain in the plane-strain direction. It can be observed that after a pre-strain along the plane-strain condition, the forming limit curve moves up for all deformation modes except plane-strain. Therefore, however, pre-strain along the ($\rho = 0$) improves the forming limits, FLC0 remains almost unchanged. The curves with pentagonal markers in *Fig. 7* illustrate the predicted FLC of AA5182-0 sheet specimens pre-loaded to $\varepsilon_1 = 0.1$ and 0.2 in equi-biaxial tension direction. It was found that the formability of the limit strains that are on the left side of the intersection increases remarkably, but the forming limits of the other part of the FLC decrease and shift toward the right side of the curve.

In *Fig. 7*, the path dependency of the FLC can be observed by considering various pre-strains. According to the above discussions, the forming limit strains are strongly path dependent, and the loading path plays an important role in the prediction of them, which means the pre-strain can shift the Forming limit strain curve in the strain space and improve the formability of the metal sheet. Also, it was seen that the strain path dependence of limit strains under bilinear loading paths with higher pre-strains is more obvious. Therefore, the larger the pre-strain, the more influence it has on the forming limits.

4.2 | Stress-Based Forming Limit Diagram

The FLSC is the Diagram of major stress (σ_1) versus minor stress (σ_2). FLSC cannot be obtained directly from experimental results, even for the uniaxial tensile test. Therefore, the theoretical calculation of the FLSC is so important and widely used in industrial metal forming processes. According to some studies, the most significant characteristic of the forming limit stress diagram is its strain path independent property. However, more recent research points out that changes in the loading path can cause some path dependency of the forming limit stress curves. In the following subsections, the sensitivity of limit stresses to the loading path will be discussed.

4.2.1 | Influences of different strain hardening models on the path dependence of the FLSC

To investigate the path dependence of the forming limit curve in stress space, the Kim-Tuan and modified Kim-Tuan strain hardening laws are chosen. Also, the Yld2000-2d yield function is utilized to study the sensitivity of limit stresses to the strain path. *Fig. 8* indicates the computed FLSC under various quantities of pre-strain along uniaxial tension for two different hardening models.

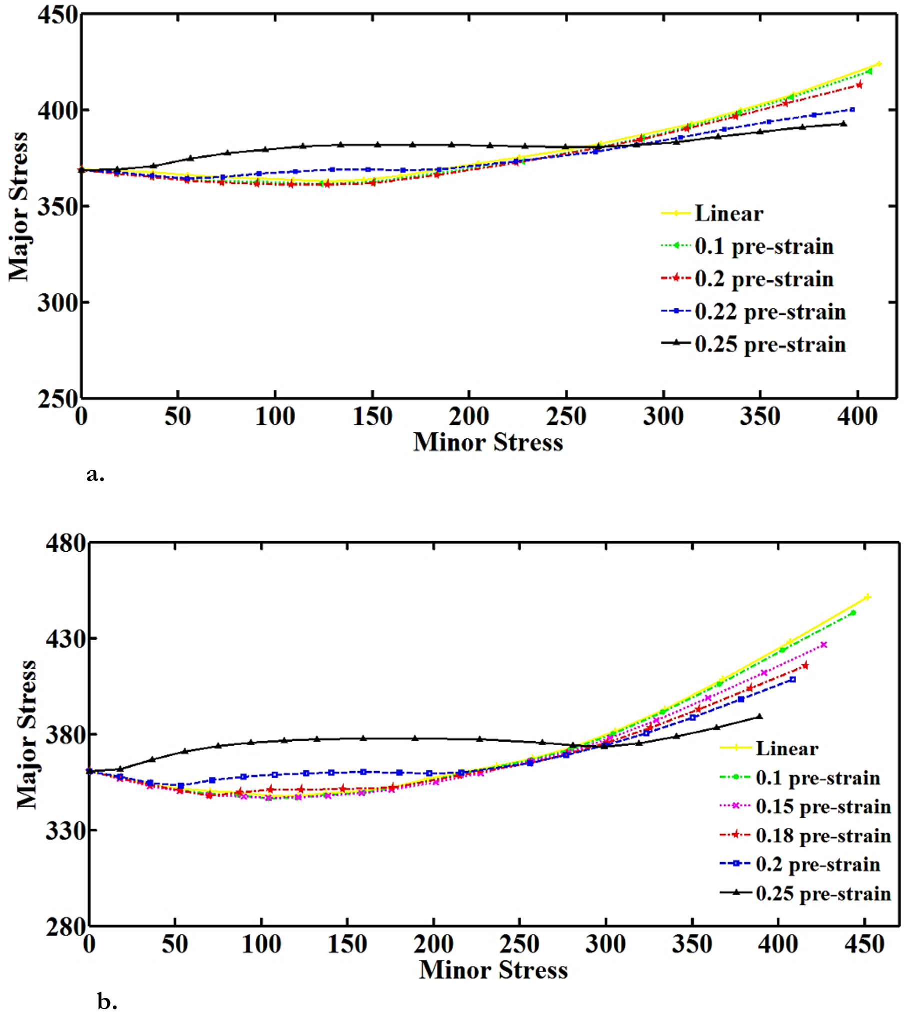

Fig. 8. Calculated FLSCs under different pre-effective strains in uniaxial tension direction by using a. Kim-Tuan, and b modified Kim-Tuan hardening laws.

The FLSC under pre-effective strains $\bar{\varepsilon} = 0.1, 0.15, 0.18, 0.2$, and 0.25 by using the Kim-Tuan work hardening law are illustrated in *Fig. 8a*. It can be seen that there is no significant difference between diagrams under pre-strains $\bar{\varepsilon} = 0.1$ and 0.15 and the linear condition. However, the FLSC obtained after $\bar{\varepsilon} = 0.18, 0.2$, and 0.25 pre-strain in uniaxial tension is significantly different.

Then, the FLSC was calculated by the modified Kim-Tuan model after $\bar{\varepsilon} = 0.1,\ 0.2, 0.22$, and 0.25 pre-effective strains in the uniaxial tension direction. As indicated in *Fig. 8.b*, no strain path dependency was observed for pre-strains $\bar{\varepsilon} = 0.1$ and 0.2. Also, plotted diagrams show FLSC after $\bar{\varepsilon} = 0.1$ and 0.2 pre-strains almost coincide with the original FLSC, but pre-strains $\bar{\varepsilon} = 0.22$ and 0.25 created significant curves.

The criterion for this behavior (dependence or independence of FLSC) is the magnitude of pre-effective strain compared to the value of the effective forming limit strain in a plane strain state and linear loading condition (effective FLC0). As indicated in *Fig. 5*, different work hardening models create different limit strains and FLC0, and also an effective FLC0. Briefly, if effective pre-strain in the multistep loading path process is less than this critical value, the final limit stresses will coincide with the FLSC in the linear condition. However, if the strain path changed after this critical value, the limit stresses will be affected by the pre-strain.

According to the above, for nonlinear loading paths with pre-effective strain less than the limit effective strain in a plane strain state, FLSC is path independent and appropriate for industrial applications, and for multi-stage processes with pre-strain larger than the critical effective strain, FLSC will be path dependent. For a detailed examination, the effective plastic forming limit curve of the AA5182-0 according to the Kim-Tuan and modified Kim-Tuan models is plotted in *Fig. 9*. As illustrated, in most regions of the Diagram, the effective limit strains based on the modified Kim-Tuan are higher than those of the Kim-Tuan model. Also, the effective FLC0 for the modified Kim-Tuan model is larger than that of the Kim-Tuan model.

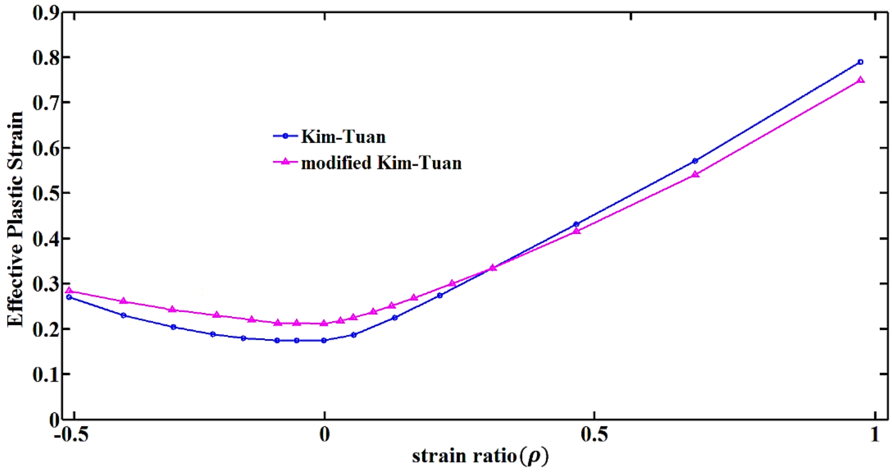

Fig. 9. Effective plastic forming limit diagrams in linear strain condition by using different hardening models.

Results indicate that the chosen strain hardening model has a great influence on the critical effective strain, and also on the path dependence of FLSC. Hence, this critical value is very important, and the magnitude of that for different hardening laws must be calculated. In fact, in this section, the effect of various stress-strain relationships on the path dependence of the FLSC by computing the critical strains is investigated. The effective FLC0 for the Kim-Tuan and modified Kim-Tuan strain hardening laws were determined, and they are equal to 0.175 and 0.212, respectively. Accordingly, FLSC is path independent with a larger pre-strain value based on the modified Kim-Tuan law than the Kim-Tuan hardening model.

The reason for this behavior is a difference in the magnitude of the effective FLC0 for these various hardening models. Therefore, the predicted FLSC by using the modified Kim-Tuan can be independent in the larger pre-strain than the Kim-Tuan model. Also, since the path dependence of FLSC is related to the value of the limit effective strain in plane strain, the accuracy of the FLC0 is very important. As shown in Fig. *5*, the modified Kim-Tuan model can predict the FLC0 with good accuracy, and the Kim-Tuan model underestimates the FLC0. Therefore, the modified Kim-Tuan hardening model is a better hardening law to estimate the path independence of the FLSC than the Kim-Tuan model.

4.2.2 | Influences of different yield functions on the path dependence of the FLSC

To survey the influence of yield criteria on the sensitivity of the forming limit stress curves to the strain path, Gotoh and Yld2000-2d functions using the modified Kim-Tuan strain hardening laws are applied. *Fig. 10* presents the forming limit stresses for various pre-effective strains in the uniaxial tension direction, considering different yield functions.

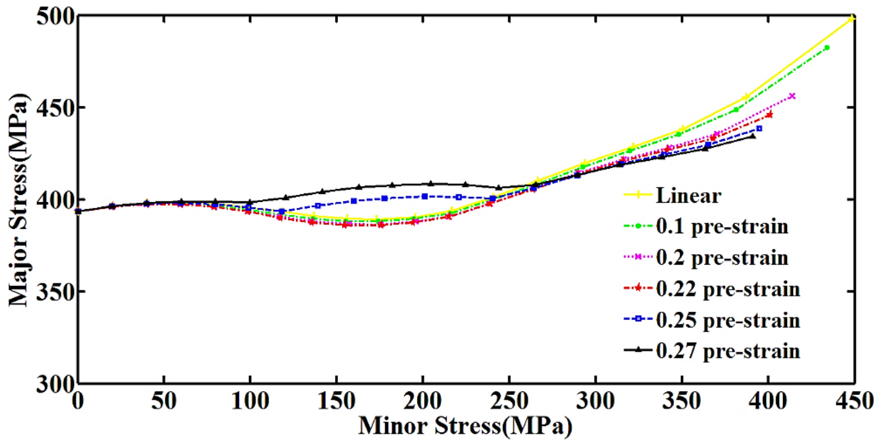

a.

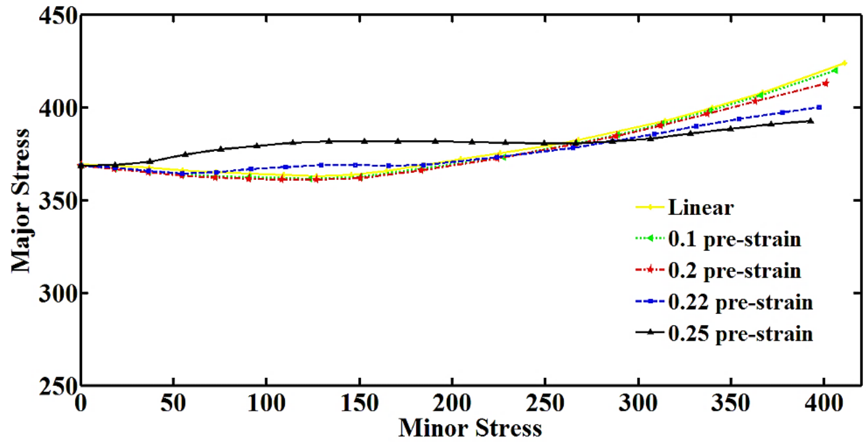

b.

Fig. 10. Calculated FLSCs under different pre-effective strains in uniaxial tension direction by using a. Gotoh, and b. Yld2000-2d yield functions.

Fig. 10.a shows the calculated limit stresses under $\bar{\varepsilon} = 0.1, 0.2, 0.22, 25$ and 0.27 pre-effective strains for the Gotoh yield function. As indicated, the FLSC obtained after pre-strains $\bar{\varepsilon} = 0.1, 0.2,$ and 0.22 almost coincides with the Diagram in the linear path condition and creates a narrow band. Only the forming stresses after pre-strains $\bar{\varepsilon} = 0.25$ and 0.27 generate a significant curve for this criterion.

Fig. 10.b demonstrates the FLSC under pre-effective strains $\bar{\varepsilon} = 0.1, 0.2, 0.22,$ and 0.25 along uniaxial tension for the Yld2000-2d yield function. Difference between the path dependency of Yld2000-2d and Gotoh yield function related to the limit stresses after pre-strain 0.22. Unlike the Yld2000, Gotoh didn't show any sensitivity to the strain path after pre-strain 0.22. This behavior can be explained by comparing the magnitude of the effective limit strains in the linear loading path condition, as shown in *Fig. 11*. The values of the effective FLC0 for Gotoh and Yld2000-2d yield criteria based on the modified Kim-Tuan model are 0.227 and 0.212. Therefore, the limit stresses by using the Gotoh function for pre- effective strain 0.22 are path independent, and by Yld2000-2d are path dependent.

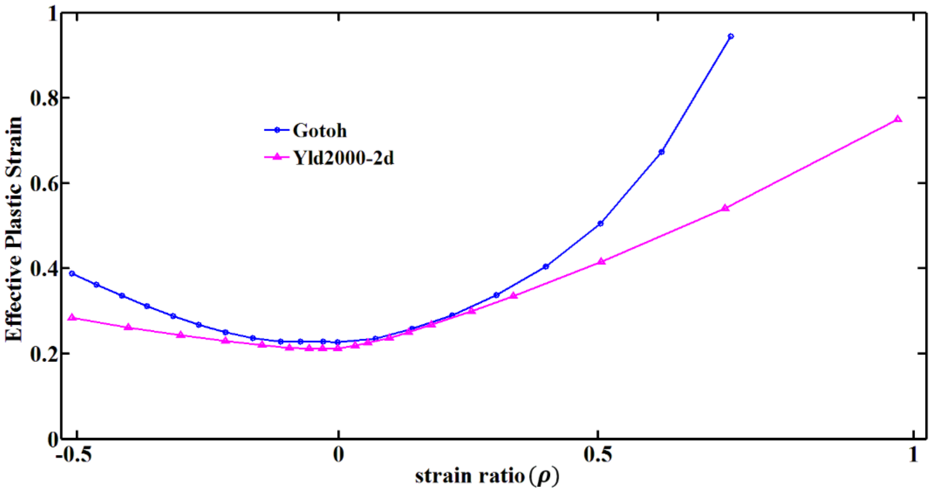

Fig. 11. Effective plastic forming limit diagrams in linear strain condition by using different yield criteria.

As discussed earlier, for small values of pre-strain, the FLSC is path independent, but if the pre-major strain increases to the effective FLC0 value, the strain path affects the FLSC. As indicated in *Fig. 8* and *Fig. 10*, the sensitivity of the forming limit stress diagram to the strain path leads to an upward shift in the limit stresses in the vicinity of the plane strain condition. The results demonstrated that selected yield criteria similar to the hardening model can affect the path dependency of the FLSC, and all of these results were concluded from the shape of the forming limit diagram of each yield function.

5 | Conclusion

Theoretical forming limit curves were obtained by using the M-K instability theory, Gotoh and Yld2000-2d yield functions based on different hardening models. Then, to prove the accuracy of theoretical FLCs, the calculated limit strains were verified with the experimental results. The comparison among them demonstrated that applying the suitable constitutive equations can considerably improve the precision of the forming limits.

The other factor that should be considered to determine an accurate Diagram, especially in a complex deformation, is the strain path. Forming limits in bilinear loading path conditions were calculated, and it was found that the path dependency of the forming limit strains is more than the forming limit stresses. Then, the path dependence of the FLSC by considering hardening models and yield functions was examined in detail. The most important consequences of this study are the following:

I. The Gotoh and Yld2000-2d yield functions are selected to study the influences of different yield criteria on forming limit diagrams. The results indicated that, however, both functions can estimate the yield behavior of the AA5182-0 alloy; there are significant differences between predicted limit strains according to them, and the Yld2000-2d gives the best prediction for experimental results.

II. It was concluded that the FLC obtained by Swift, Kim-Tuan, and modified Kim-Tuan models provides a good fit with experimental data according to the Yld2000-2d yield function. Also, the Modified Kim-Tuan strain hardening law calculated the more precisely forming limit strains for AA5182-0 sheet than other hardening laws.

III. The FLC in nonlinear strain path processes is significantly dependent on the strain path. Although the sensitivity of forming limits in stress space to loading path is less than limit strains, FLSC is not completely path independent.

IV. The forming limit curves in stress space for the multistep strain path processes will be path independent if the pre-strain is less than the effective FLC0. Therefore, if the pre-strain is larger than the critical effective limit strain, the limit stresses will be sensitive to the loading path.

V. Results indicated that the selective hardening model and yield function significantly affect the path dependency of the forming limit stress curve. Since different constitutive models create various critical effective FLC0, the sensitivity of FLSC to strain path will be changed by applying the different hardening models.

Conflict of Interest

The authors declare no conflict of interest.

Data Availability

All data are included in the text.

Funding

This research received no specific grant from funding agencies in the public, commercial, or not-for-profit sectors.

References

[1] Keeler, S. P. (1961). Plastic instability and fracture in sheets stretched over rigid punches [Thesis]. https://dspace.mit.edu/handle/1721.1/120282

[2] Goodwin, G. M. (1968). *Application of strain analysis to sheet metal forming problems in the press shop*. https://doi.org/10.4271/680093

[3] Marciniak, Z., & Kuczyński, K. (1967). Limit strains in the processes of stretch-forming sheet metal. *International journal of mechanical sciences*, *9*(9), 609–620. https://doi.org/10.1016/0020-7403(67)90066-5

[4] Butuc, M. C., Banabic, D., da Rocha, A. B., Gracio, J. J., Duarte, J. F., Jurco, P., & Comsa, D. S. (2002). The performance of Yld96 and BBC2000 yield functions in forming limit prediction. *Journal of Materials Processing Technology*, *125*, 281–286. https://doi.org/10.1016/S0924-0136(02)00399-0

[5] Wu, P. D., Jain, M., Savoie, J., MacEwen, S. R., Tuğcu, P., & Neale, K. W. (2003). Evaluation of anisotropic yield functions for aluminum sheets. *International journal of plasticity*, *19*(1), 121–138. https://doi.org/10.1016/S0749-6419(01)00033-X

[6] Barlat, F., Brem, J. C., Yoon, J. W., Chung, K., Dick, R. E., Lege, D. J., …& Chu, E. (2003). Plane stress yield function for aluminum alloy sheets—part 1: Theory. *International journal of plasticity*, *19*(9), 1297–1319. https://doi.org/10.1016/S0749-6419(02)00019-0

[7] Ganjiani, M., & Assempour, A. (2007). An improved analytical approach for the determination of forming limit diagrams considering the effects of yield functions. *Journal of Materials Processing Technology*, *182*(1–3), 598–607. https://doi.org/10.1016/j.jmatprotec.2006.09.025

[8] Pham, Q. T., Lee, B. H., Park, K. C., & Kim, Y. S. (2018). Influence of the post-necking prediction of hardening law on the theoretical forming limit curve of aluminium sheets. *International journal of mechanical sciences*, *140*, 521–536. https://doi.org/10.1016/j.ijmecsci.2018.02.040

[9] Pham, Q. T., Lee, M. G., & Kim, Y. S. (2019). Characterization of the isotropic-distortional hardening model and its application to commercially pure titanium sheets. *International journal of mechanical sciences*, *160*, 90–102. https://doi.org/10.1016/j.ijmecsci.2019.06.023

[10] Mirfalah-Nasiri, S. M., Basti, A., & Hashemi, R. (2016). Forming limit curves analysis of aluminum alloy considering the through-thickness normal stress, anisotropic yield functions, and strain rate. *International journal of mechanical sciences*, *117*, 93–101. https://doi.org/10.1016/j.ijmecsci.2016.08.011

[11] Nasiri, S. M. M., Basti, A., Hashemi, R., & Darvizeh, A. (2018). Effects of normal and through-thickness shear stresses on the forming limit curves of AA3104-H19 using advanced yield criteria. *International journal of mechanical sciences*, *137*, 15–23. https://doi.org/10.1016/j.ijmecsci.2018.01.009

[12] Hou, Z., Liu, Z., Wan, M., Wu, X., Yang, B., & Lu, X. (2020). An investigation on the anisotropic behavior and forming limit of 5182-H111 aluminum alloy. *Journal of materials engineering and performance*, *29*(6), 3745–3756. https://doi.org/10.1007/s11665-020-04879-7

[13] Wang, C., Yi, Y., Huang, S., Dong, F., He, H., Huang, K., & Jia, Y. (2021). Experimental and theoretical investigation on the forming limit of 2024-O aluminum alloy sheet at cryogenic temperatures. *Metals and materials international*, *27*(12), 5199–5211. https://doi.org/10.1007/s12540-020-00922-3

[14] Uppaluri, R., & Helm, D. (2021). A convex fourth-order yield function for orthotropic metal plasticity. *European journal of mechanics-a/solids*, *87*, 104196. https://doi.org/10.1016/j.euromechsol.2020.104196

[15] Graf, A., & Hosford, W. (1994). The influence of strain-path changes on forming limit diagrams of A1 6111 T4. *International journal of mechanical sciences*, *36*(10), 897–910. https://doi.org/10.1016/0020-7403(94)90053-1

[16] Yoshida, K., Kuwabara, T., & Kuroda, M. (2007). Path-dependence of the forming limit stresses in a sheet metal. *International journal of plasticity*, *23*(3), 361–384. https://doi.org/10.1016/j.ijplas.2006.05.005

[17] Yoshida, K., & Kuwabara, T. (2007). Effect of strain hardening behavior on forming limit stresses of steel tube subjected to nonproportional loading paths. *International journal of plasticity*, *23*(7), 1260–1284. https://doi.org/10.1016/j.ijplas.2006.11.008

[18] Nurcheshmeh, M., & Green, D. E. (2011). Investigation on the strain-path dependency of stress-based forming limit curves. *International journal of material forming*, *4*(1), 25–37. https://doi.org/10.1007/s12289-010-0989-4

[19] Wang, H., Yan, Y., Han, F., & Wan, M. (2017). Experimental and theoretical investigations of the forming limit of 5754O aluminum alloy sheet under different combined loading paths. *International journal of mechanical sciences*, *133*, 147–166. https://doi.org/10.1016/j.ijmecsci.2017.08.040

[20] Zhalehfar, F., Hashemi, R., & Hosseinipour, S. J. (2015). Experimental and theoretical investigation of the strain path change effect on the forming limit diagram of AA5083. *The international journal of advanced manufacturing technology*, *76*(5), 1343–1352. https://doi.org/10.1007/s00170-014-6340-3

[21] Sojodi, S., Basti, A., Falahatgar, S. R., & Nasiri, S. M. M. (2021). Investigation on the forming limit diagram of AA5754-O alloy by considering the strain hardening model, strain path, and through-thickness normal stress. *The international journal of advanced manufacturing technology*, *113*(9), 2495–2511. https://doi.org/10.1007/s00170-021-06801-4

[22] Nguyen, H. H., & Vu, H. C. (2020). Forming limit prediction of anisotropic aluminum magnesium alloy sheet AA5052-H32 using micromechanical damage model. *Journal of materials engineering and performance*, *29*(7), 4677–4691. https://doi.org/10.1007/s11665-020-04987-4

[23] Sener, B., Kilicarslan, E. S., & Firat, M. (2020). Modelling anisotropic behavior of AISI 304 stainless steel sheet using a fourth-order polynomial yield function. *Procedia manufacturing*, *47*, 1456–1461. https://doi.org/10.1016/j.promfg.2020.04.320

[24] Wang, Y., Zhang, C., Wang, Y., Zhao, G., & Chen, L. (2021). An investigation on the anisotropic plastic behavior and forming limits of an Al-Mg-Li alloy sheet. *Journal of materials engineering and performance*, *30*(11), 8224–8234. https://doi.org/10.1007/s11665-021-05981-0

[25] Barlat, F., Yoon, J. W., & Cazacu, O. (2007). On linear transformations of stress tensors for the description of plastic anisotropy. *International journal of plasticity*, *23*(5), 876–896. https://doi.org/10.1016/j.ijplas.2006.10.001

[26] Aretz, H., & Barlat, F. (2013). New convex yield functions for orthotropic metal plasticity. *International journal of nonlinear mechanics*, *51*, 97–111. https://doi.org/10.1016/j.ijnonlinmec.2012.12.007

[27] Da Rocha, A. B., Barlat, F., & Jalinier, J. M. (1985). Prediction of the forming limit diagrams of anisotropic sheets in linear and nonlinear loading. *Materials science and engineering*, *68*(2), 151–164. https://doi.org/10.1016/0025-5416(85)90404-5

Appendix A

Hill constant parameters identification: material coefficients for the Hill48 yield function are determined by using the r-value in different directions as follows [22]:

$$\mathrm{F}=\frac{\mathrm{r}_0}{\mathrm{r}_{90}(1+\mathrm{r}_0)}, \qquad \mathrm{G}=\frac{1}{1+\mathrm{r}_0}, \tag{A1}$$

$$H = \frac{r_0}{1+r_0}, \qquad N = \frac{(1+2r_{45})(r_0+r_{90})}{2r_{90}(1+r_0)}.$$

The values of the anisotropic r-value are given in *Table 1*.

Appendix B

Gotoh constant parameters identification: the coefficients of the Gotoh yield function are obtained by using the direct approach as follows [14]:

$$\begin{aligned}
&A_1 = 1, \quad A_2 = -\frac{4r_0}{1+r_0}, \quad A_4 = -\frac{4r_{90}}{1+r_{90}}\left(\frac{\sigma_0}{\sigma_{90}}\right)^4, \quad A_5 = \left(\frac{\sigma_0}{\sigma_{90}}\right)^4, \\
&A_3 = \left(\frac{\sigma_0}{\sigma_b}\right)^4 - (A_1 + A_2 + A_4 + A_5), \quad A_9 = \frac{16r_{45}}{1+r_{45}}\left(\frac{\sigma_0}{\sigma_{45}}\right)^4 + \left(\frac{\sigma_0}{\sigma_b}\right)^4, \\
&A_6 = \frac{1+5r_0}{1+r_0} + 4\left(\frac{\sigma_0}{\sigma_{45}}\right)^4 - \left(\frac{\sigma_0}{\sigma_{90}}\right)^4, \quad A_8 = \frac{1+5r_{90}}{1+r_{90}}\left(\frac{\sigma_0}{\sigma_{90}}\right)^4 + 4\left(\frac{\sigma_0}{\sigma_{45}}\right)^4 - 1, \\
&A_7 = \frac{16}{1+r_{45}}\left(\frac{\sigma_0}{\sigma_{45}}\right)^4 - 2\left(\frac{\sigma_0}{\sigma_b}\right)^4 - A_6 - A_8.
\end{aligned} \tag{B1}$$

The values of the experimental quantities $r_0,\ r_{45},\ r_{90},\ r_b,\ \sigma_0,\ \sigma_{45}, \sigma_{90}, \sigma_b$ are given in *Table 1*.

Appendix C

Yld2000-2d constant parameters identification: to determine the yield functions constants, the values of the r-values and flow stresses in $0°, 45°$, and $90°$ direction from rolling ($r_0, r_{45}, r_{90}, \sigma_0, \sigma_{45}, \sigma_{90}$), should be applied in the following equations [13]:

$$F = \phi - 2\left(\frac{\bar{\sigma}}{\sigma}\right)^a = 0, \tag{C1}$$

$$G = q_x \frac{\partial \phi}{\partial s_{xx}} - q_y \frac{\partial \phi}{\partial s_{yy}} = 0, \tag{C2}$$

where q_x and q_x are the functions of the r-values, also γ and δ are constant values listed in *Table 4*. Substituting *Eq. (4)* into *Eq. (C1)* and *Eq. (C2)* leads to:

$$F_J = \left|\alpha_1\gamma_J - \alpha_2\delta_J\right|^a + \left|\alpha_3\gamma_J + 2\alpha_4\delta_J\right|^a + \left|2\alpha_5\gamma_J + \alpha_6\delta_J\right|^a - 2\left(\frac{\bar{\sigma}}{\sigma_J}\right)^a = 0, \tag{C3}$$

$$F_4 = \left|\frac{\sqrt{x_2'^2 + 4\alpha_7^2}}{2}\right|^a + \left|\frac{3x_1'' - \sqrt{x_2''^2 + 4\alpha_8^2}}{4}\right|^a + \left|\frac{3x_1'' + \sqrt{x_2''^2 + 4\alpha_8^2}}{4}\right|^a - 2\left(\frac{\bar{\sigma}}{\sigma_{45}}\right)^a = 0, \tag{C4}$$

$$\begin{aligned}
G_J = {} & \left(\alpha_1 q_{xJ} + \alpha_2 q_{yJ}\right)\left(\alpha_1\gamma_J + \alpha_2\gamma_J\right)\left|\alpha_1\gamma_J + \alpha_2\gamma_J\right|^{a-2} \\
& + \left(\alpha_3 q_{xJ} - 2\alpha_4 q_{yJ}\right)\left(\alpha_3\gamma_J + 2\alpha_4\delta_J\right)\left|\alpha_3\gamma_J + 2\alpha_4\delta_J\right|^{a-2} \\
& + \left(2\alpha_5 q_{xJ} - \alpha_6 q_{yJ}\right)\left(2\alpha_5\gamma_J + \alpha_6\delta_J\right)\left|2\alpha_5\gamma_J + \alpha_6\delta_J\right|^{a-2} = 0,
\end{aligned} \tag{C5}$$

$$G_4 = \bar{V}'\frac{x_2'^2}{\sqrt{x_2'^2 + 4\alpha_7^2}} + \frac{3}{2}x_1''(\bar{V}'' + \bar{W}'') + \frac{1}{2}\frac{x_2''^2}{\sqrt{x_2''^2 + 4\alpha_8^2}}(\bar{W}'' - \bar{V}'') - \frac{2a}{1+r_{45}}\left(\frac{\bar{\sigma}}{\sigma_{45}}\right)^a = 0, \tag{C6}$$

where:

$$x'_1 = \frac{\alpha_1 + \alpha_2}{3}\ , \quad x'_2 = \frac{\alpha_1 - \alpha_2}{3}. \tag{C7}$$

$$x''_1 = \frac{\alpha_3 + 2\alpha_4 + 2\alpha_5 + \alpha_6}{9}\ , \quad x''_2 = \frac{2\alpha_5 + \alpha_6 - \alpha_3 - 2\alpha_4}{3}. \tag{C8}$$

$$\bar{V}' = a\left(\frac{\sqrt{x'^2_2 + 4\alpha_7^2}}{2}\right)^{a-1}. \tag{C9}$$

$$\bar{V}'' = a\left(\frac{3x''_1 - \sqrt{x''^2_2 + 4\alpha_8^2}}{4}\right)\left|\frac{3x''_1 - \sqrt{x''^2_2 + 4\alpha_8^2}}{4}\right|^{a-2}. \tag{C10}$$

$$\bar{W}'' = a\left(\frac{3x''_1 + \sqrt{x''^2_2 + 4\alpha_8^2}}{4}\right)\left|\frac{3x''_1 + \sqrt{x''^2_2 + 4\alpha_8^2}}{4}\right|^{a-2}. \tag{C11}$$

According to the above equations, there is a system of eight equations to determine the eight anisotropic coefficients of the Yld2000-2d yield function [25]. The Newton-Raphson method is performed to minimize the error function, and the constant parameters are determined.

Appendix D

Kim-Tuan coefficients identification: constant parameters of the Kim-Tuan hardening model are computed according to the following equations [8]:

$$t_k = \frac{5}{\varepsilon^*}. \tag{D1}$$

$$h_k = \frac{\sigma^*}{\sigma^* - \sigma_0}(\varepsilon^* + \varepsilon_0). \tag{D2}$$

$$K_k = \frac{\sigma^* - \sigma_0}{(\varepsilon^* + \varepsilon_0)^{\sigma^*(\varepsilon^*+\varepsilon_0)/(\sigma^*-\sigma_0)}}. \tag{D3}$$

The point $(\varepsilon^*, \sigma^*)$ is the Maximum Tensile Force Point (MTFP).

Appendix E

Newton-Raphson method: this method is used to solve the N functional equations to find the variable x_i, where $i = 1,2, ..., N$, as below:

$$F_i(x_1, x_1, \dots, x_N) = 0\ , \ \ i = 1,2, \dots, N. \tag{E1}$$

values of x_i are shown as vector x and functions F_i are defined as F. According to the Taylor series, functions F_i in the neighborhood of the x are written as follows:

$$F_i(x + \delta x) = F_i(x) + \sum_{j=1}^{N} \frac{\partial F_i}{\partial x_j}\delta x_j + O(\delta x^2). \tag{E2}$$

This matrix is rewritten in the form of a Jacobian matrix (J):

$$F(x + \delta x) = F(x) + J.\delta x + O(\delta x^2). \tag{E1}$$

$$J_{ij} = \frac{\partial F_i}{\partial x_j}. \tag{E4}$$

Since $F(x + \delta x) = 0$, by neglecting the $\delta x^2 = 0$ in *Eq. (E3)*, a set of equation are obtained:

$$J.\,\delta x = -F \Longrightarrow \delta x = -J^{-1}.\,F. \qquad \textbf{(E5)}$$

The δx are added to the old value as:

$$x_{new} = x_{old} + \delta x. \qquad \textbf{(E6)}$$

The iterative processes are repeated to minimize the error functions and converge to the point.